

## Realistic Detection and Early Warning of Binary Neutron Stars with Decihertz Gravitational-wave Observatories

CHANG LIU <sup>1,2</sup> YACHENG KANG <sup>1,2</sup> AND LIJING SHAO <sup>2,3</sup>

<sup>1</sup>*Department of Astronomy, School of Physics, Peking University, Beijing 100871, China*

<sup>2</sup>*Kavli Institute for Astronomy and Astrophysics, Peking University, Beijing 100871, China*

<sup>3</sup>*National Astronomical Observatories, Chinese Academy of Sciences, Beijing 100012, China*

(Received June 1, 2022; Revised June 1, 2022; Accepted June 1, 2022)

Submitted to ApJL

### ABSTRACT

We investigated the detection and localization of binary neutron star (BNS) populations with decihertz gravitational-wave observatories in a realistic detecting strategy, including real-time observations and early warnings. Assuming 4 years' operation of B-DECIGO, we found that the detected BNSs can be divided into three categories: (a) sources that merge within 1 year, which could be localized with an uncertainty of  $\Delta\Omega \sim 10^0 \text{ deg}^2$ ; (b) sources that merge in 1–4 years, which take up three quarters of the total events and yield the most precise angular resolution with  $\Delta\Omega \sim 10^{-2} \text{ deg}^2$  and time-of-merger accuracy with  $\Delta t_c \sim 10^{-1} \text{ s}$ ; and (c) sources that do not merge during the 4-yr mission window, which enable possible early warnings, with  $\Delta\Omega \sim 10^{-1} \text{ deg}^2$  and  $\Delta t_c \sim 10^0 \text{ s}$ . Furthermore, we compared the pros and cons of B-DECIGO with the Einstein Telescope, and explored the prospects of detections using 3 other decihertz observatories and 4 BNS population models. In realistic observing scenarios, we found that decihertz detectors could even provide early-warning alerts to a source decades before its merger while their localizations are still more accurate than ground-based facilities. Finally we found a decrease of events when considering the confusion noise, but this could be partially solved by a proper noise subtraction.

*Keywords:* Gravitational wave astronomy (675) – Neutron stars (1108) – Gravitational wave detectors (676)

### 1. INTRODUCTION

The detection of gravitational waves (GWs) from the binary neutron star (BNS) inspiral GW170817 has opened an exciting era of multi-messenger astronomy (Abbott et al. 2017a,b). In combination with the following electromagnetic (EM) counterparts, joint detection of BNS mergers by GW and EM facilities provided us unprecedented opportunities to explore many fundamental questions (Sathyaprakash et al. 2019), including dense matter properties in extreme conditions with associated high-energy astrophysical processes (Abbott et al. 2017c, 2018), tests of general relativity in the strong-field regime (Abbott et al. 2017d, 2019a), and the cosmic expansion with the “standard siren” technique (Schutz 1986; Abbott et al. 2017e).

The prerequisite for a successful multi-messenger detection is the prompt communication of source location and other properties from GW data to EM telescopes. For GW170817, the short  $\gamma$ -ray burst (GRB), GRB 170817A, was observed  $\sim 1.7 \text{ s}$  after the BNS merger, while the localization from LIGO/Virgo took hours (Abbott et al. 2017d). People have been studying and improving the low-latency GW triggers (Hooper et al. 2012; Nitz et al. 2018; Abbott et al. 2019b). They have also assessed the detection and early warning abilities for compact binary mergers observed by current and future ground-based GW detectors, including LIGO, Virgo, and KAGRA (Abbott et al. 2020), as well as the third-generation detectors, the Einstein Telescope (ET) and Cosmic Explorer (CE; see e.g., Sachdev et al. 2020; Nitz & Dal Canton 2021; Singh et al. 2021; Magee & Borhanian 2022; Borhanian & Sathyaprakash 2022).

While the real-time detections and early warnings from ground-based GW detectors have been closely examined, less attention has been paid to decihertz space-based GW detec-

tors. Current research on BNS detections with decihertz detectors focuses on the prospects of detection rates with GW lensing effects (Piórkowska-Kurpas et al. 2021), cosmology with simplified detection strategies (Seto et al. 2001; Geng et al. 2020; Cao et al. 2022), and parameter estimations of representative sources (Isoyama et al. 2018; Nakano et al. 2021). However, there are few studies on the realistic detection of BNS population and their early warnings from decihertz GW detectors (Liu & Shao 2022).

Decihertz space-based GW detectors have a distinct advantage over ground-based ones, for which the GW signals from BNS systems could stay days to years in the decihertz band (Isoyama et al. 2018). By virtue of this, decihertz detectors can observe sources that are not only about to merge, but also solely in the inspiral stage for the duration of observation. For such sources, decihertz detectors could gather enough information from their pre-merger stages and provide the locations and times of merger in advance to EM facilities. As we will see, even after the detectors end their missions, their legacies on source information remain valuable for early warnings for a couple of years.

What a pre-merger alert needs most is the information of source location and time of merger. Liu & Shao (2022) have shown that the angular resolution depends on the detector’s trajectory baseline and the orientation of the source. Grover et al. (2014) have shown that the time of merger accuracy scales inversely with the detector frequency bandwidth and signal-to-noise ratio (SNR). However, different signal durations, population distributions, and detector designs make this problem more complex.

The aim of this paper is to extend early studies on decihertz BNS early warnings by simulating detections in real observing scenarios, and exploring the distributions of the accuracy in localization and timing. In this work, using the Fisher information matrix (Finn 1992), we investigate the realistic detections and early warnings of 4 BNS population models with 4 representative decihertz GW observatories. In addition, we also compare their detection performances with the ET, and discuss the influence of the confusion noise.

The paper is organized as follows. In Sec. 2, we introduce the population models, detectors, and the detecting strategy. In Sec. 3, taking B-DECIGO (Kawamura et al. 2021) and one population model as an example, we illustrate typical observational characteristics of sources. We found that BNS sources in decihertz GW detectors can be divided into 3 categories with distinct abilities in providing location and timing information. Section 4 compares the predictions from B-DECIGO with that from ET, and Secs. 5 and 6 compare the detection prospects using other decihertz detectors and other population models, respectively. In Sec. 7, we briefly discuss the influence of the GW foreground from compact binaries on detection rates. Section 8 concludes the study.

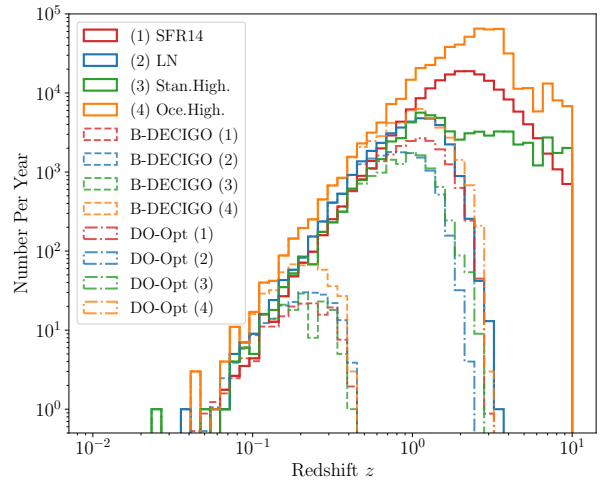


**Figure 1.** Solid histograms show the total number of BNSs per year from population models. Dashed and dash-dotted histograms show sources that will merger in the fourth year of a 4-yr mission, to be detected by B-DECIGO and DO-Optimal, respectively.

Appendices give more information on the merger rate calculation and GW foreground from unresolved double compact objects. Throughout this paper, we use geometrized units in which  $G = c = 1$ .

## 2. SETTING

In this section, we will introduce the BNS population models (Sec. 2.1) and decihertz detectors (Sec. 2.2) that we adopted in this work, as well as the detecting strategy of BNSs (Sec. 2.3).

### 2.1. BNS population models

For the cosmic evolution of BNS merger rate, there are various types of population models (for a review, see Mandel & Broekgaarden 2022). In our work, we have implemented 4 representative classes of them. Their distributions are given in Fig. 1 with solid histograms, and the models—abbreviated as “SFR14”, “LN”, “Stan.High”, and “Oce.High”—are introduced as follows:

- (1) **SFR14**—We assumed that the merger rate evolves with redshift following the fitting formula of star formation rate (SFR) from Madau & Dickinson (2014), and we adopted a local merger rate  $\mathcal{R}_0 = 44 \text{ Gpc}^{-3} \text{ yr}^{-1}$  based on the “PDB (ind)” model which is informed by events in the third GW transient catalog (GWTC-3) of compact binary mergers (Abbott et al. 2021).
- (2) **LN**—Many population models are constructed based on a delay time superposed on the SFR, such as the Gaussian delay model, power-law delay model (Virgili et al. 2011), and log-normal delay model (Wanderman & Piran 2015).

According to the observations of short GRBs, log-normal delay model is favored (Sun et al. 2015). We adopted the dimensionless redshift distribution of the log-normal delay model in Eq. (A8) of Zhu et al. (2021), and a local merger rate  $\mathcal{R}_0 = 44 \text{ Gpc}^{-3} \text{ yr}^{-1}$ .

- (3) **Stan.High**—We adopted the “Stan.High” and “Oce.High” models from Dominik et al. (2013).<sup>1</sup> These models have been applied in many other studies (Dominik et al. 2015; Ding et al. 2015; Piórkowska-Kurpas et al. 2021). “Stan.High” is the standard model with a “high-end” metallicity evolution.
- (4) **Oce.High**—“Oce.High” is the “Optimistic common envelope” model with a “high-end” metallicity evolution (Dominik et al. 2013).

Although different population models evolve differently with redshift, most of the population synthetic codes start with the SFR of Madau & Dickinson (2014) and some of them have similar evolving trends (Baibhav et al. 2019). Therefore, similarly to Nitz & Dal Canton (2021), we choose SFR14 as our fiducial model. Without specific mention, our calculations are based on it. Our redshift cutoff is at  $z = 10$  and we transform redshift to luminosity distance  $D_L$  based on the  $\Lambda$ CDM model with the matter density parameter  $\Omega_M = 0.315$ , the dark-energy density parameter  $\Omega_\Lambda = 0.685$ , and the Hubble constant  $H_0 = 67.4 \text{ km s}^{-1} \text{ Mpc}^{-1}$  (Aghanim et al. 2020).

We focus on a typical BNS system where the two component masses,  $M_1$  and  $M_2$ , are both  $1.4 M_\odot$ . According to Nitz & Dal Canton (2021), the localization results can be rescaled to apply to sources with other masses or local merger rates. For other parameters, we choose the dimensionless tidal deformability  $\tilde{\Lambda} = 675$ , the spins of neutron stars  $\chi_{1,2} = 0$ , the source direction angles,  $\cos \theta_S \in \mathcal{U}(-1, 1)$  and  $\phi_S \in \mathcal{U}(0, 2\pi)$ , and the angular momentum direction angles,  $\cos \theta_L \in \mathcal{U}(-1, 1)$  and  $\phi_L \in \mathcal{U}(0, 2\pi)$ , where  $\mathcal{U}(\cdot, \cdot)$  denotes a uniform distribution.

### 2.2. Decihertz GW detectors

We use 4 space-based decihertz GW detectors to explore their performance: (i) the baseline mission B-DECIGO (Isoyama et al. 2018; Kawamura et al. 2021), (ii) the full-scale mission DECIGO (Yagi & Seto 2011; Kawamura et al. 2011), (iii) a conservative example DO-Conservative, and (iv) an optimal example DO-Optimal (Sedda et al. 2020, 2021). The sensitivity curves of them are plotted in Fig. 2 and readers are referred to Sec. 2.2 of Liu & Shao (2022) for details. To compare the detection prospects with the next-generation ground-based GW detectors, we will use ET (Hild et al. 2011) as an example, whose noise curve is also shown in Fig. 2.

### 2.3. Detecting strategy

After the launch of a space-based GW detector, the observing time grows with its operation time until the mission ends, which we conservatively set as 4 years. During the mission time, two kinds of BNSs could be observed: the one that will merge within the mission time and the one that only inspirals throughout these years. For the inspiral signals, they exist in the data for the whole 4 years; for the merger signals, they exist in the data for 0 to 4 years depending on their merger time. We denote the time from the start of the mission to the merger of a BNS as  $t_{c_0}$ . Based on the observational properties, notably—of our interests here—the localization and timing accuracy, we classify the BNS sources into 3 categories:

- (a) BNSs that merge within 1 year ( $t_{c_0} \leq 1 \text{ yr}$ );
- (b) BNSs that merge in 1 to 4 years ( $1 \text{ yr} < t_{c_0} \leq 4 \text{ yr}$ );
- (c) BNSs that only inspiral within the whole 4-yr observational span ( $t_{c_0} > 4 \text{ yr}$ ).

We use “(a)”, “(b)”, and “(c)” to denote these categories, and they are annotated in Fig. 2 for a BNS signal at  $z = 0.02$ .

Assuming BNS systems will merge following the prediction of a population model, every year there will be approximately the same amount of merger signals. Contrary to short-lived signals received by ground-based hectohertz GW detectors, these signals could however exist in space-based decihertz GW detectors from the start of the mission to the merger or to the end of the mission. Except for those merger signals that are observed within only the first few days of the mission, all the signals will exist in decihertz detectors long enough to guarantee a relatively stable parameter estimation precision, especially for localization. Figure 7 in Liu & Shao (2022) has shown that, for long-lasting signals, localization precision makes no difference whether we end the observations a few hours or a few days before the merger. Therefore for decihertz space-based detectors, “early warning” is time-independent to a certain extent. They can always provide accurate localization and time of merger to both GW and EM detectors for followups. For signals in category (c), space-based detectors could even provide “legacy” information after they stop operating.

Our calculation is performed as follows. For every week, from the start of the mission to 20 years after it, we generate BNS sources according to the population model. Then we calculate their parameter precisions by the Fisher matrix method following the setup in Liu & Shao (2022) with slight revisions: parameters used in the Fisher information matrix are  $\Xi = \{\mathcal{M}, \eta, t_c, \phi_c, D_L, \bar{\theta}_S, \bar{\phi}_S, \bar{\theta}_L, \bar{\phi}_L\}$ , where  $\mathcal{M}$  is the chirp mass;  $\eta$  is the symmetric mass ratio;  $\phi_c$  and  $t_c$  are the phase and time at the coalescence. Our attention focuses on the estimation of the accuracy of angular resolution,  $\Delta\Omega$ , and time of merger,  $\Delta t_c$ . SNR threshold for detection is set to be

<sup>1</sup> <https://www.syntheticuniverse.org>

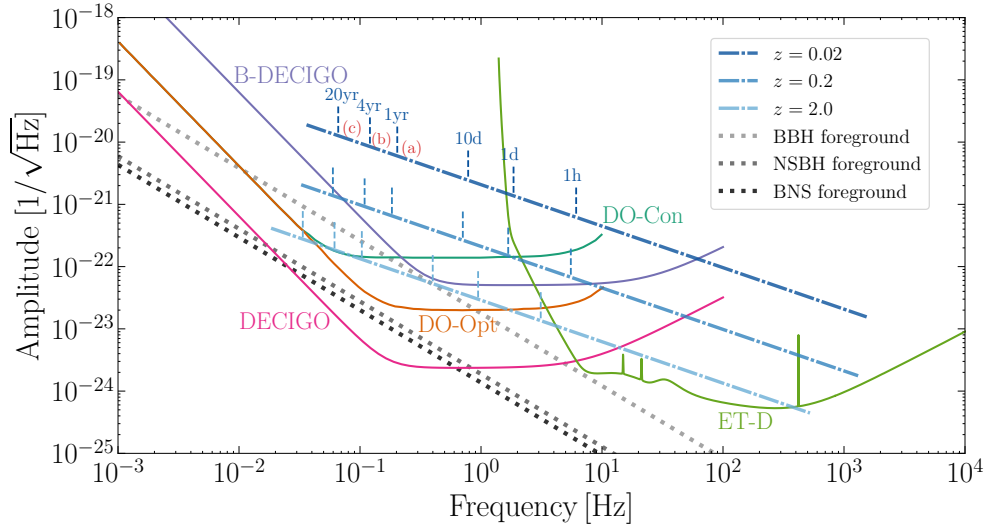


**Figure 2.** The amplitude of the sources and detector noises. The sky-averaged effective noise  $\sqrt{S_n^{\text{eff}}(f)}$  of various detectors [see Eq. (29) of Liu et al. (2020)] is given in solid lines; the pre-subtracted BNS/NSBH/BBH foregrounds from model “Stan.High” are given in dashed grey lines; the simulated BNS signals,  $2\sqrt{f}|\tilde{h}_+(f)|$ , at redshift  $z = 0.02, 0.2$ , and  $2.0$  are illustrated with dash-dotted blue lines. Source signals are plotted with a duration of 100 years. For each source, the short dashed vertical lines mark the times before coalescence. Categories (a), (b), and (c) are annotated on the illustrated source at  $z = 0.02$ .

8. During the calculation of the SNR and the Fisher matrix, we need to calculate the inner product, which is an integration in the frequency domain, from  $f_{\text{in}}$  to  $f_{\text{out}}$ . As a BNS is to merge in time  $t_{c_0}$ , we have  $f_{\text{in}} = (t_{c_0}/5)^{-3/8} M^{-5/8}/8\pi$ . For categories (a) and (b), we set  $f_{\text{out}} = f_{\text{high}}$  being the frequency upper limit of the detector, while for category (c) we set  $f_{\text{out}} = [(t_{c_0} - 4 \text{ yr})/5]^{-3/8} M^{-5/8}/8\pi$ .

Note that we generate BNS sources weekly so that a shorter sampling period would cause large fluctuations in event numbers, and a longer sampling period would lead to a biased parameter estimation result. Also note that the event numbers may be decimals due to normalization. Namely, following the evolution of each population model, we simulate plenty of sources by adjusting  $\mathcal{R}_0$  in Eq. (A1), and when presenting the results we normalize to the model’s local merger rate, e.g.,  $\mathcal{R}_0 = 44 \text{ Gpc}^{-3} \text{ yr}^{-1}$  for the “SFR14” model. It is referred as “normalized simulation” in later sections.

### 3. CHARACTERISTICS OF BNSS IN THREE CATEGORIES

In this section, taking the detector B-DECIGO and population model “SFR14” as an example, we present different characteristics with categories (a), (b), and (c) defined in Sec. 2.3. The main conclusion of our findings is that, the statistical properties of accuracy in localization and time of merger for these 3 categories have distinct and unique features, and it is better to consider them separately when studying them.

Before discussing categories (a), (b), and (c) separately, we first introduce some characteristics in our figures and tables. Figure 3 shows the weekly and yearly detection rates of the BNSs, while Table 1 records the yearly detections. Those

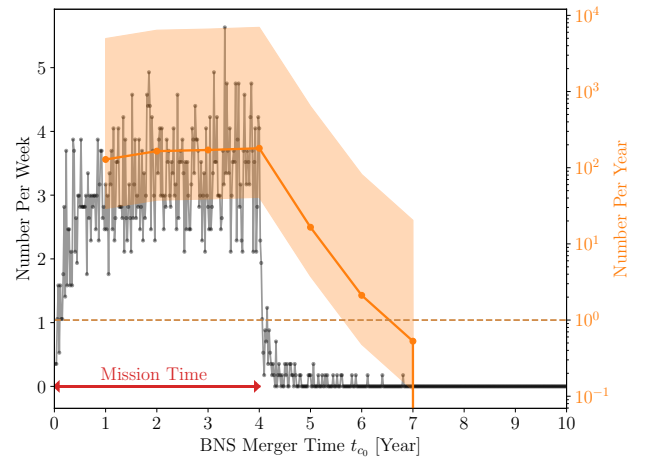


**Figure 3.** Black symbols show the detection number per week for B-DECIGO as a function of BNS merger time  $t_{c_0}$  since the observation starts. We assume that the mission lasts for 4 years, and have used the population model “SFR14”. The orange dots and shaded area, with labels on the right hand side, indicate respectively the yearly detection number and the range of BNS local merger rate inferred from GWTC-3, namely in the range of  $[10, 1700] \text{ Gpc}^{-3} \text{ yr}^{-1}$  (Abbott et al. 2021). The dashed horizontal brown line gives a yearly detection of only 1 BNS. Sources that cannot merge within 7 years after the launch of B-DECIGO could not be detected.

results are based on normalized simulations. Figures 4 and 5, on the other hand, show the distributions of the BNS sources from a single simulation, i.e., using  $\mathcal{R}_0 = 44 \text{ Gpc}^{-3} \text{ yr}^{-1}$  directly. Note that we calculate all the sources with  $t_{c_0} \leq 20 \text{ yr}$ , but for B-DECIGO, no sources could be detected if  $t_{c_0} \gtrsim 7 \text{ yr}$ ,

**Table 1.** Event numbers detected by 4 decihertz GW detectors for different observation periods since the start of the observation. The percentage in the brackets shows the ratio of it to the total number of detections in 20 yrs. We have used the ‘‘SFR14’’ population model.

Detector	$z_{\max}$	$t_{c_0} \in (0, 1]$ yr	$t_{c_0} \in (1, 2]$ yr	$t_{c_0} \in (2, 3]$ yr	$t_{c_0} \in (3, 4]$ yr	$t_{c_0} \in (4, 5]$ yr	$t_{c_0} \in (5, 10]$ yr	$t_{c_0} \in (10, 20]$ yr
B-DECIGO	$\sim 0.45$	128 (19%)	165 (25%)	171 (26%)	180 (27%)	16.5 (2.5%)	2.64 (0.4%)	0 (0%)
DO-Conservative	$\sim 0.26$	10.4 (3.7%)	25.8 (9.3%)	36.8 (13%)	50.5 (18%)	32.0 (11%)	70.5 (25%)	53.0 (19%)
DO-Optimal	$\sim 3.0$	9610 (13%)	17200 (23%)	19400 (25%)	20400 (27%)	5620 (7.4%)	3230 (4.2%)	535 (0.7%)
DECIGO	$> 10$	175000 (15%)	175000 (16%)	175000 (16%)	175000 (16%)	140000 (12%)	223000 (20%)	66700 (5.9%)

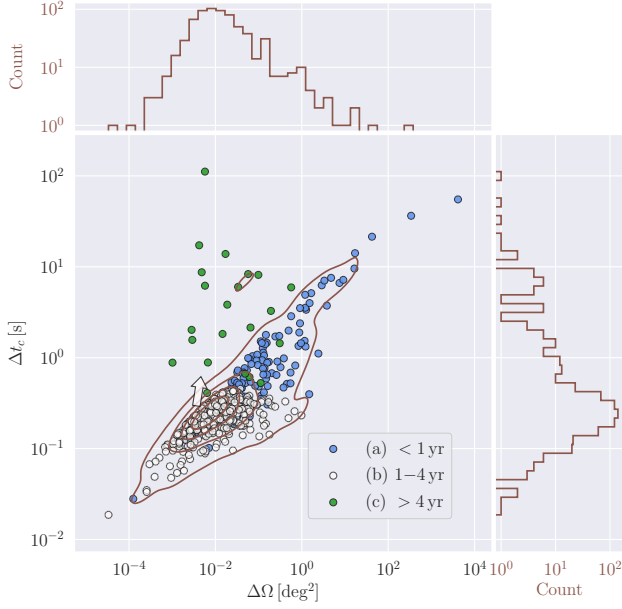


**Figure 4.** The  $\Delta\Omega$ - $\Delta t_c$  distribution of the sources that could be detected during the operation of B-DECIGO. Population model ‘‘SFR14’’ is adopted. The categories (a), (b), and (c) are plotted in blue, white, and green circles, respectively. The white arrow shows the direction in which the parameter precision of category (b) moves, if early warning is required. The 4 brown contour lines delimit 5 iso-proportions of the number density.

namely sources that enter the observational window when they have more than 7 years to coalesce.

For BNSs in category (a), their signals only stay shortly ( $\leq 1$  yr) in B-DECIGO. As a result, not enough information could be accumulated by the detector to enable precise parameter estimation. Figure 3 shows that the weekly number of detections ( $\text{SNR} > 8$ ) increases gradually from less than one to about 4, then becomes stable. Meanwhile, from Figs. 4 and 5 we see that  $\Delta t_c$  and  $\Delta\Omega$  from  $t_{c_0} = 0$  to  $t_{c_0} = 1$  yr have an improvement of 3 to 4 orders of magnitude. The reason for localization accuracy can be explained by the trajectory baseline of the detector, which is short at the beginning of the mission, leading to an inaccurate sky localization in category (a).

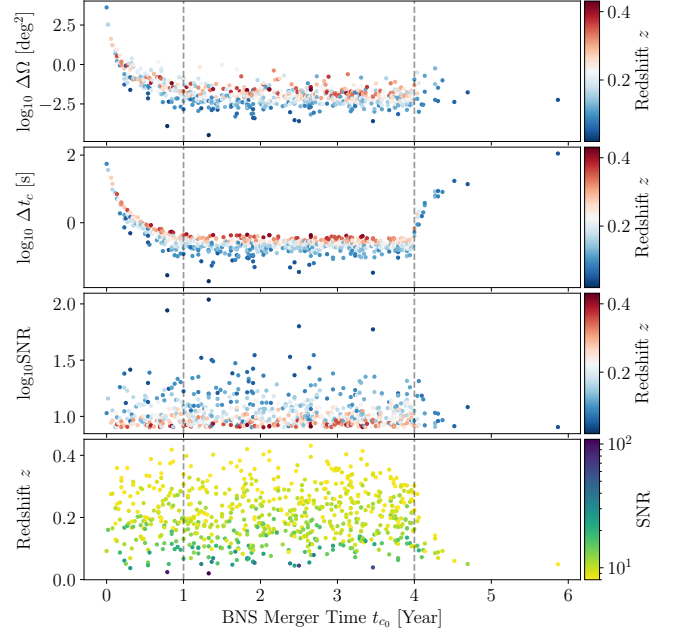


**Figure 5.** The angular resolution (*top*), time of merger accuracy (*second panel*), SNR (*third panel*), and redshift (*bottom*) of the sources detected by B-DECIGO as a function of  $t_{c_0}$ . The dots are plotted weekly since the calculation is performed with such a cadence. Colors indicate the redshift or SNR of these sources. Two vertical dashed lines divide BNSs into, from left to right, categories (a), (b), and (c).

The majority of the detectable BNS sources in B-DECIGO belong to category (b), which yields the best and most stable parameter estimation results. From Table 1 we notice that the yearly detection rate of this category is more than that of category (a), and the entire category (b) takes up 78% of the total detections. From the middle parts of Fig. 5 ( $1 \text{ yr} < t_{c_0} \leq 4 \text{ yr}$ ) and the white circles in Fig. 4 we find that the angular resolutions and timing accuracies are clustered around  $\Delta\Omega \sim 10^{-2} \text{ deg}^2$  and  $\Delta t_c \sim 0.1 \text{ s}$ . Such a steady distribution is unrelated to the integration time, which is the reason why we consider all the BNSs that merge within 1 to 4 years into this category. Note that we derive our results by integrating to  $f_{\text{out}} = 100 \text{ Hz}$ , which is  $\sim 2 \text{ s}$  before the actual final merger. If one wants parameter estimation results from days earlier

to execute the early warning alerts, the white arrow on Fig. 4 shows the direction of the changes. We also find that the SNR and redshift distributions are similar for both categories (a) and (b), where sources up to  $z = 0.45$  can be detected.

Category (c) contains a special kind of BNSs from space-based detectors. The prominent feature of category (c) is that only nearby sources from us could be observed, judging from the last panel of Fig. 5 when  $t_{c_0} > 4$  yr. Another feature is that the timing accuracy  $\Delta t_c$  drops rapidly to  $\sim 10^2$  s in category (c). The reason would be a lack of information due to a short integration interval in the frequency band, which is caused by the quasi-monochromatic waves emitted by the sources that are far from their merger stage. However, although the precision of  $\Delta t_c$  in category (c) is relatively poor, it is still useful in most cases. The  $\Delta\Omega$  in this category is only slightly less accurate than in category (b), with a mean value of  $0.1 \text{ deg}^2$ . The baseline of B-DECIGO in the Earth orbit from a 4-yr continuous observation gives rise to such accuracy. For BNSs in this category, with such accurate localization, joint detections from both EM and ground-based GW searches would be still promising.

For B-DECIGO, only  $\sim 3\%$  of the detected sources belong to category (c), and it cannot detect sources with  $t_{c_0} \gtrsim 7$  yr because of its decreased sensitivity at  $0.1 \text{ Hz}$ . This non-detection problem does not exist in other decihertz GW detectors such as DO-Conservative, for which  $\sim 50\%$  of the detectable sources are in category (c). We will discuss this point in Sec. 5.

As we will see later, the typical detection features of the sources in categories (a), (b), and (c) have the similar patterns, regardless of changes in detectors (or sensitivity curves) and population models. Their relative positions on a  $\Delta\Omega$ - $\Delta t_c$  plot are similar to those in Fig. 4 and the evolution trends of the observables with source merger time  $t_{c_0}$  are similar to those in Fig. 5, while only the numbers of detections and absolute precisions alter.

#### 4. COMPARISONS WITH ET

In this section, in order to illustrate the pros and cons of space-based decihertz GW detectors, we compare  $\Delta\Omega$ ,  $\Delta t_c$ , and SNR of the BNS sources to be detected by B-DECIGO with that of the ET, the proposed European next-generation ground-based GW detector (Kalogera et al. 2021).

When a BNS signal enters ground-based detectors, the merger phase becomes prominent, such that the effective tidal deformability parameter  $\tilde{\Lambda}$  and the effective spin parameter  $\chi_s$  become important to the GW phase evolution. Therefore we also consider these parameters in the calculations of ET (see e.g., Gao et al. 2022; Liu & Shao 2022).

Figure 6 compares the results from B-DECIGO with that of ET. From the first panel, we notice that the SNRs in ET are a few times higher than that of B-DECIGO, which means

that all the BNSs detected by B-DECIGO could be identified by ET when they merge, regardless of their merger time  $t_{c_0}$ . This is especially true for sources in category (c) because they are much closer to us than sources from other categories. In spite of this, from the second panel we find that the  $\Delta\Omega$  from B-DECIGO is actually 1 to 4 orders of magnitude better than ET, especially in categories (b) and (c). This characteristic is of great use to multi-messenger astronomy because the localizations from ground-based GW detectors alone are not accurate enough to guarantee the detections of all kinds of EM follow-ups. The merger time uncertainty  $\Delta t_c$  is larger for B-DECIGO than ET. However, B-DECIGO's sub-second errors on  $t_c$  are already sufficient for the preparation of EM observations, not to mention the long enough early warning time from B-DECIGO that the ground GW detectors cannot provide.

Note that the above analyses only compare the results from ET to that of B-DECIGO. Other decihertz detectors such as DO-Optimal and DECIGO could detect sources further than ET (see Table 1). More details are given in the next section, but the general trend that space-based decihertz detectors have better localization ability and worse time of merger accuracy stays the same.

#### 5. OTHER DECIHERTZ DETECTORS

We begin by analyzing the common features. Figure 7 shows the yearly numbers of detections from DO-Conservative, DO-Optimal, and DECIGO. A summary is given in Table 1. We notice that all these three detectors could observe sources with  $t_{c_0}$  up to 20 yr, since they all have a lower noise level at the frequency range of BNS inspirals for sources in category (c). The numbers of detections, however, vary significantly due to different levels of the total noise.

Figure 8 shows the probability distributions of the redshift  $z$ , SNR,  $\Delta t_c$ , and  $\Delta\Omega$  from the 4 decihertz detectors. The top panel shows the distributions of the redshift and we also record the largest redshift  $z_{\text{max}}$  in Table 1. Instead of using the sky-averaged estimations, our recorded  $z_{\text{max}}$  takes into consideration of the directional dependency of the source, therefore it represents the farthest horizon distance. We also calculated the sky-averaged ones and their redshifts are few times smaller (e.g.,  $z_{\text{max}}^{\text{ave}} \sim 1.0$  for DO-Optimal), which indicates that in real observations, we could detect sources much further than the averaged estimations.

From the last two panels in Fig. 8 we find that the categories (a), (b), and (c) are more dominant than the detector sensitivity in determining the distributions of  $\Delta t_c$  and  $\Delta\Omega$ . In categories (b) and (c),  $\Delta\Omega$  of the sources is always less than  $O(1) \text{ deg}^2$ , regardless of the qualities of the detectors, and the timing accuracies of most sources in categories (c) are  $\Delta t_c > 1$  s. However, the ranges of the parameter precisions span orders of magnitude depending on specific detector designs.

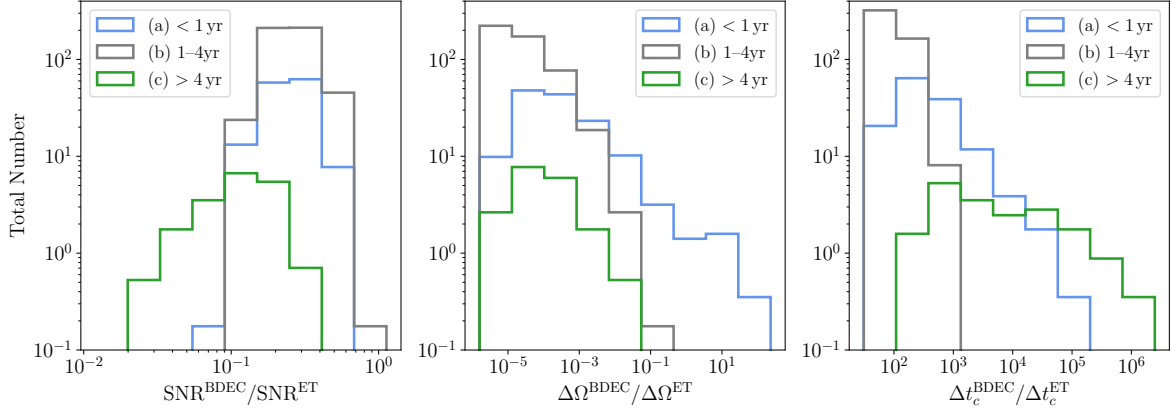


**Figure 6.** Distributions of the ratios of SNR (*left*), angular resolution (*middle*) and accuracy in the time of merger (*right*), for the sources to be detected by B-DECIGO over that by ET. Sources in categories (a), (b), and (c) are given in blue, grey, and green histograms, respectively.

We now explore the specialties of decihertz GW detectors one by one. Compared to B-DECIGO, DO-Conservative has a higher noise level at  $f > 0.2$  Hz, leading to a significant drop in the number of detections. The weekly detection rates hardly reach one. However, DO-Conservative has a better sensitivity at lower frequencies, which greatly boosts the number of detections in categories (b) and (c), especially in category (c). Thus, it can observe sources that will merge more than dozens of years after the mission ends. Exclusive characteristics for DO-Conservative could be found in Figs. 9 and 11.

Using DO-Optimal, the weekly detection rates of the sources with  $t_{c_0} < 4$  yr gradually increase, from 0 to 400, but then drop drastically in category (c). Approximately 2 years after the detector closes down, the weekly number of detections falls to be fewer than 10. Though DO-Optimal is an upgraded version of DO-Conservative, the parameter distributions for both of them are similar, judging from Fig. 8. Exclusive characteristics for DO-Optimal could be found in Figs. 10 and 12.

DECIGO is the most powerful detector in the decihertz band that we consider. Except for the first  $\sim 10$  weeks, DECIGO will detect all the merger signals within 4 years, i.e., signals from both categories (a) and (b). Meanwhile, because of its full design with a very high sensitivity, both categories (a) and (b) have the same level of localization and timing abilities, which are orders of magnitude more accurate than the other three detectors.

## 6. OTHER POPULATION MODELS

In Fig. 1 we have presented the redshift distributions of the 4 BNS population models, as well as the distributions of the merger events detected by B-DECIGO and DO-Optimal in their last year of operation ( $3 \text{ yr} < t_{c_0} \leq 4 \text{ yr}$ ) for each population model.

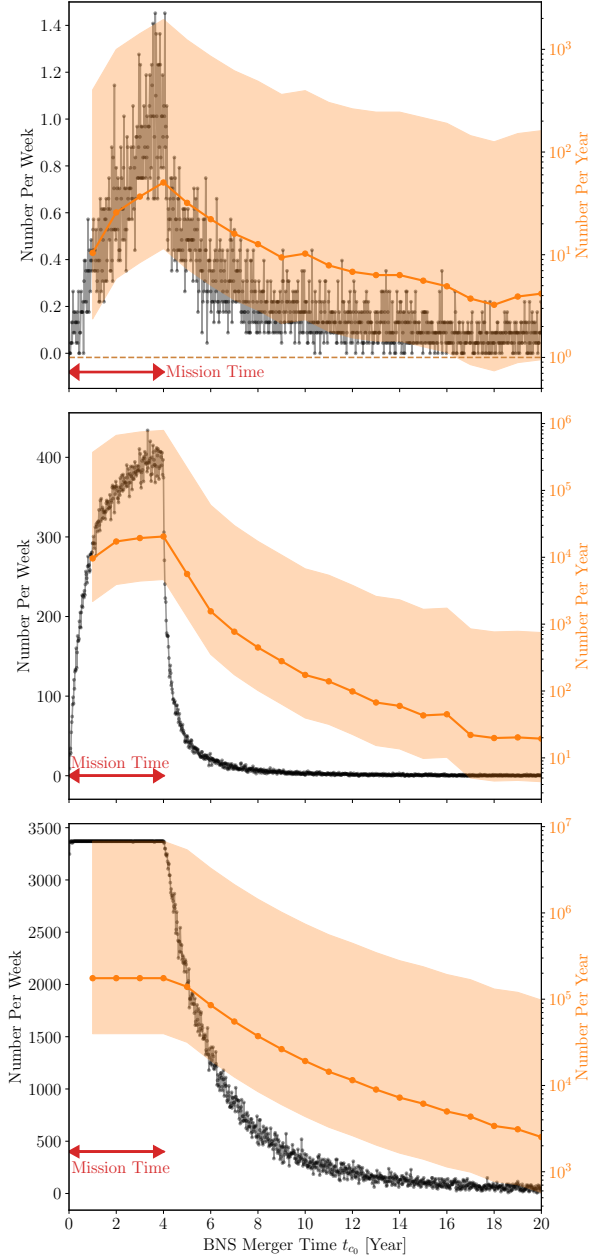
We find that though different populations could be clearly distinguished by their original redshift distributions, it is hard

for us to tell the differences among the distributions of the detectable sources—they are unlike the original distributions due to the horizon distance of B-DECIGO and DO-Optimal. A dedicated Bayesian analysis might be able to give confident inference to them. Model “Oce.High” has the largest number of sources, leading to the largest detection number for both detectors, which makes it easily recognized. Models “SFR14”, “LN”, and “Stan.High”, however, could not be distinguished by B-DECIGO. The horizon distance of B-DECIGO is  $z_{\text{max}} \sim 0.45$  while sources from these three models have similar distributions before  $z = 1$ . However, after  $z = 1$ , the number of mergers for model “SFR14” raises, while for models “LN” and “Stan.High”, it drops sharply and remains stable, respectively. Such characteristics are conducive to DO-Optimal, whose horizon could reach  $z_{\text{max}} \sim 3$ . As expected, for DO-Optimal, sources detected from model “SFR14” outnumber the other two models, whereas model “LN” has several orders of magnitude fewer detections than model “Stan.High” in the last 4 redshift bins in Fig. 1.

Note that population models “SFR14” and “LN” are scaled to the local merger rate,  $\mathcal{R}_0 = 44 \text{ Gpc}^{-3} \text{ yr}^{-1}$ , which has a relative error of up to 2 orders of magnitude by the values provided by GWTC-3 (Abbott et al. 2021). Therefore the relevant distribution and number of detections may scale accordingly.

## 7. THE IMPACT OF CONFUSION NOISE

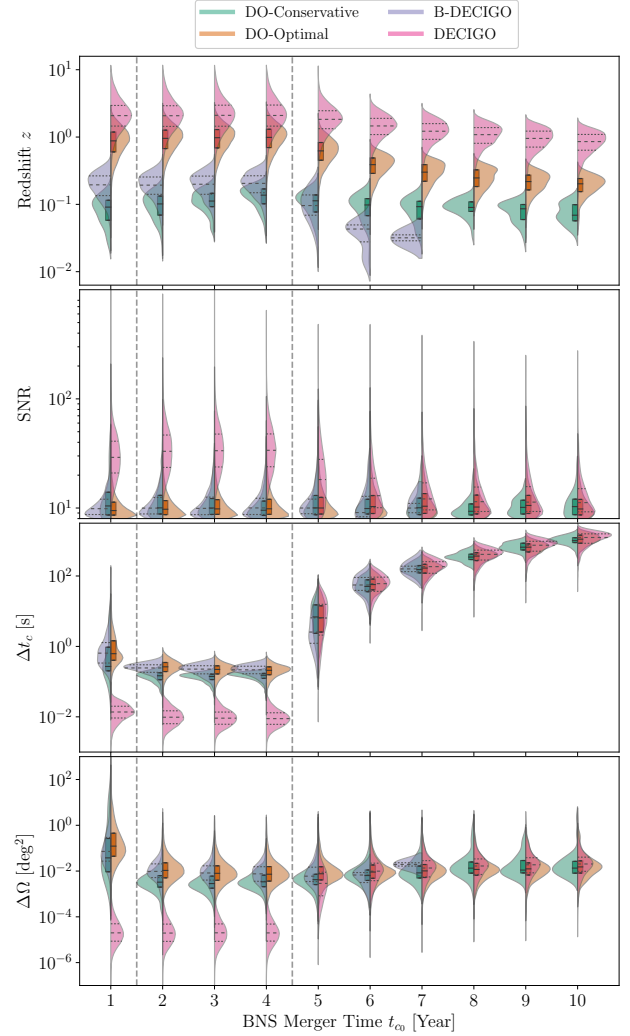
All the results above leave out the consideration of the confusion noise (Christensen 2019; Barish et al. 2021). In reality, the stochastic GWs from the undetectable sources could leave imprints in the detectors, which are determined by the fractional energy density  $\Omega_{\text{GW}}$ . The amplitude of  $\Omega_{\text{GW}}$  contributed from double compact objects (DCO) is about  $10^{-12}$ – $10^{-9}$  at 1 Hz depending on the population properties. It transforms to the confusion noise shown in the grey dotted lines in Fig. 2. Appendix B shows the details of calculation.



**Figure 7.** Same as Fig. 3, for DO-Conservative (*top*), DO-Optimal (*middle*), and DECIGO (*bottom*).

It has been shown that, the confusion noise from DCOs could be subtracted out by an iteration scheme and a global fit (Cutler & Harms 2006). However it depends severely on the specific population model, the sensitivity of the detector and its operation time, which leads to large uncertainties in the calculation. Nevertheless, as shown by Kudoh et al. (2006) and Yagi & Seto (2011), the full design of DECIGO is adequate for subtracting out the binary foreground.

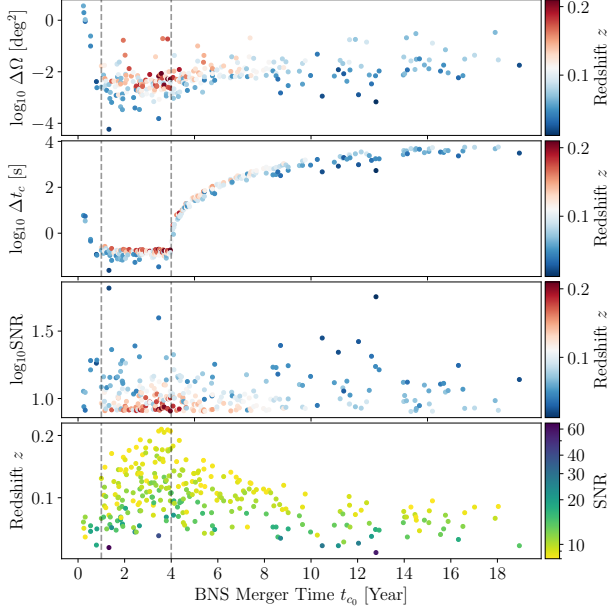
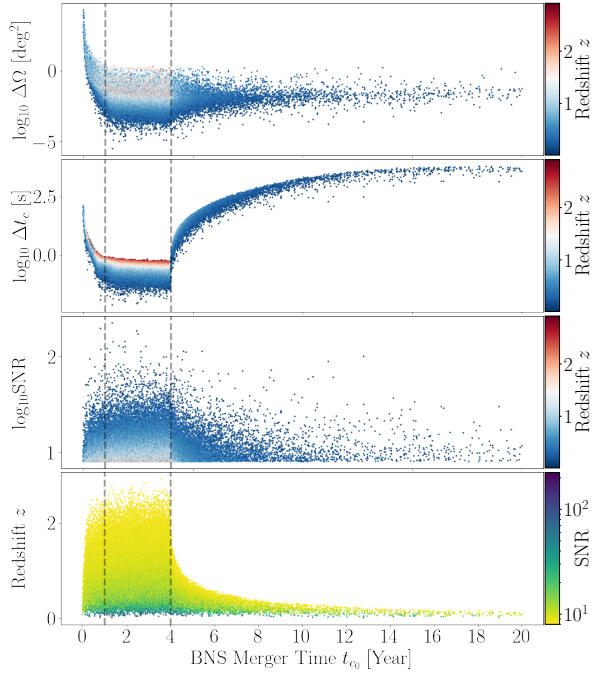
Here we take a conservative approach. We have calculated the confusion noise based on the population models imple-



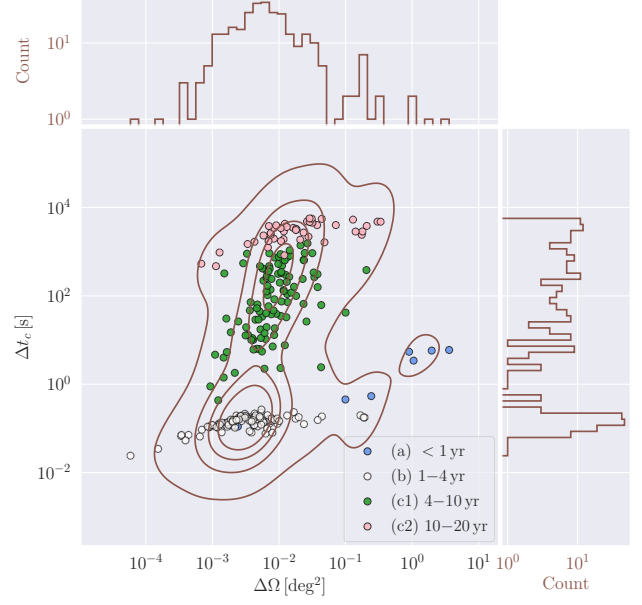
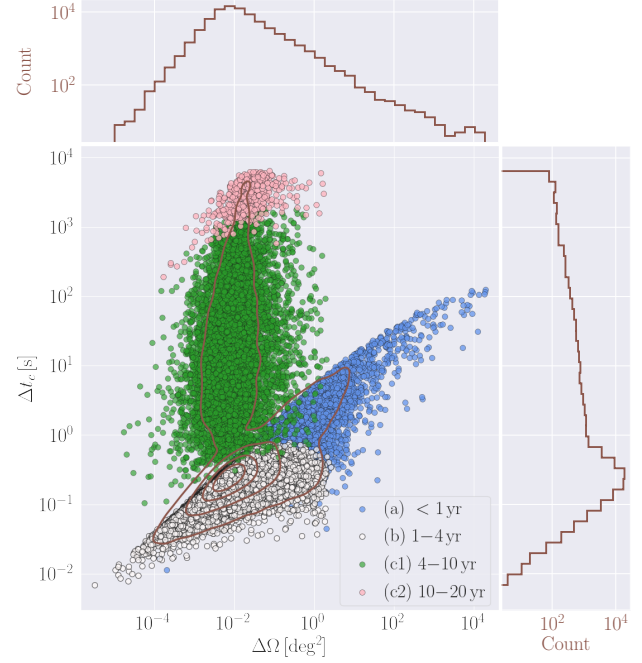
**Figure 8.** Probability distributions of redshift (*top*), SNR (*second panel*),  $\Delta t_c$  (*third panel*), and  $\Delta\Omega$  (*bottom*) of the detected sources in DO-Conservative (*green*), DO-Optimal (*orange*), B-DECIGO (*blue*), and DECIGO (*pink*) as a function of BNS merger time  $t_{c0}$ . The horizontal dashed lines and the box plots on each violin plot show the quartiles of each distribution. The original sources are generated according to the population model “SFR14” and the two vertical dashed lines divide BNSs into categories (a), (b), and (c).

**Table 2.** The yearly number of detections of the sources with  $t_{c0} < 1$  yr in category (a), with (numerator) or without (denominator) the consideration of the confusion noise from GW foreground. We show their ratios in brackets.

	B-DECIGO	DO-Conservative	DO-Optimal
SFR14	124/127 (98%)	8/8 (100%)	5600/9600 (58%)
LN	159/160 (99%)	13/13 (100%)	6700/8700 (77%)
Stan.High	51/124 (41%)	4/9 (44%)	211/6300 (3.3%)
Oce.High	48/349 (14%)	6/31 (19%)	91/22000 (0.7%)


**Figure 9.** Same as Fig. 5 for DO-Conservative.

**Figure 10.** Same as Fig. 5 for DO-Optimal.

mented in our paper (see Table 3 in Appendix B), and estimated the number of detections with or without the confusion noise in Table 2. Note that we do not include DECIGO since it can identify all the sources. We do not have estimations on  $\Omega_{\text{GW}}^{\text{NSBH}}$  and  $\Omega_{\text{GW}}^{\text{BBH}}$  for population models ‘‘SFR14’’ and ‘‘LN’’, since they are phenomenological models fitted to the observa-


**Figure 11.** Same as Fig. 4 for DO-Conservative.

**Figure 12.** Same as Fig. 4 for DO-Optimal.

tions. But for models ‘‘Stan.High’’ and ‘‘Oce.High’’, we obtain an estimation on  $\Omega_{\text{GW}}^{\text{NSBH}}$  and  $\Omega_{\text{GW}}^{\text{BBH}}$  by their NSBH/BBH population models from Dominik et al. (2013). Such a difference leads to a significant distinction in detection rates.

Table 2 presents the number of detections of the sources that will merge in the first year with or without the con-

fusion noise. Considering the subtraction scheme, the actual numbers of detections should be somewhere in between. We notice that the confusion noise purely from BNS populations only slightly affects our results, especially for B-DECIGO and DO-Conservative where the effect is smaller than 2%. However, since the BBH and NSBH foregrounds are orders of magnitude larger than that of BNSs, they will affect the numbers of detections severely. B-DECIGO and DO-Conservative will miss  $\sim 50\%$  of the detectable sources for the ‘‘Stan.High’’ model and  $\sim 80\%$  for the ‘‘Oce.High’’ model. The DCO foreground has the largest impact on DO-Optimal. Its number of detections declines drastically no matter in only the BNS foreground or the whole DCO foreground, though the absolute numbers are still greater than those of B-DECIGO and DO-Conservative.

The above results are just for a conservative reference, since we did not subtract the confusion noise due to the complexity of population models and observation periods. For detectors with closer horizon distances, such as DO-Conservative, few subtractions need to be done and our results are more likely to be close to reality.

## 8. DISCUSSIONS

We provide the detections and early warning predictions of different BNS populations to be observed by decihertz GW observatories with realistic simulations. By the Fisher matrix method, we show that the sources detected by decihertz detectors could be divided into 3 categories based on their properties on a  $\Delta\Omega$ - $\Delta t_c$  map, which is determined by the specifics of space-based heliocentric-orbit detectors. Sources in category (a) that merge quickly have less accurate localization and timing precision. Sources in category (b) that merge within 1–4 years after the launch have stable and the best parameter estimation results. Sources in category (c) that do not

merge within the mission time could still offer early warning alerts.

We demonstrate that decihertz GW detectors have, on average,  $\sim 10^3$  times better localization ability than the ET, which in general applies to all 3 categories of sources. We then compare the Monte Carlo simulation results from B-DECIGO, DO-conservative, DO-optimal, and DECIGO, and provide their numbers of detections over time. Furthermore, we provide the detection prospects for 4 different population models and discuss the influence of the confusion noise.

With such strong localization capability from decihertz space-based GW detectors, joint detections with EM telescopes and satellites become possible. Synergy observations might be carried out with, e.g., SWIFT (Gehrels et al. 2004), GECAM (Zhang et al. 2019), eXTP (in ’t Zand et al. 2019), EP (Yuan et al. 2018), THESEUS (Ciolfi et al. 2021), WFST (Shi et al. 2018), Mephisto (Lei et al. 2021), ZTF (Graham et al. 2019), and JWST (Gardner et al. 2006). For the EM facilities that have field-of-views larger than squares-of-degree level, joint detections will almost always succeed as long as EM counterparts reach above their detection thresholds. Therefore, future multi-messenger astronomy using decihertz detectors with EM followups will be very promising, and provides interesting science outcomes.

## ACKNOWLEDGEMENTS

This work was supported by the National Natural Science Foundation of China (11975027, 11991053, 11721303), the National SKA Program of China (2020SKA0120300), the Max Planck Partner Group Program funded by the Max Planck Society, and the High-Performance Computing Platform of Peking University. Y.K. acknowledges the Hui-Chun Chin and Tsung-Dao Lee Chinese Undergraduate Research Endowment (Chun-Tsung Endowment) at Peking University.

## REFERENCES

- Abbott, B. P., et al. 2017a, *PhRvL*, 119, 161101, doi: [10.1103/PhysRevLett.119.161101](https://doi.org/10.1103/PhysRevLett.119.161101)
- , 2017b, *ApJL*, 848, L12, doi: [10.3847/2041-8213/aa91c9](https://doi.org/10.3847/2041-8213/aa91c9)
- , 2017c, *ApJL*, 850, L39, doi: [10.3847/2041-8213/aa9478](https://doi.org/10.3847/2041-8213/aa9478)
- , 2017d, *ApJL*, 848, L13, doi: [10.3847/2041-8213/aa920c](https://doi.org/10.3847/2041-8213/aa920c)
- , 2017e, *Natur*, 551, 85, doi: [10.1038/nature24471](https://doi.org/10.1038/nature24471)
- , 2018, *PhRvL*, 121, 161101, doi: [10.1103/PhysRevLett.121.161101](https://doi.org/10.1103/PhysRevLett.121.161101)
- , 2019a, *PhRvL*, 123, 011102, doi: [10.1103/PhysRevLett.123.011102](https://doi.org/10.1103/PhysRevLett.123.011102)
- , 2019b, *ApJ*, 875, 161, doi: [10.3847/1538-4357/ab0e4f](https://doi.org/10.3847/1538-4357/ab0e4f)
- , 2020, *LRR*, 23, 3, doi: [10.1007/s41114-020-00026-9](https://doi.org/10.1007/s41114-020-00026-9)
- Abbott, R., et al. 2021, arXiv e-prints, arXiv:2111.03634, <https://arxiv.org/abs/2111.03634>
- Aghanim, N., et al. 2020, *Astron. Astrophys.*, 641, A6, doi: [10.1051/0004-6361/201833910](https://doi.org/10.1051/0004-6361/201833910)
- Baibhav, V., Berti, E., Gerosa, D., et al. 2019, *PhRvD*, 100, 064060, doi: [10.1103/PhysRevD.100.064060](https://doi.org/10.1103/PhysRevD.100.064060)
- Barish, B. C., Bird, S., & Cui, Y. 2021, *PhRvD*, 103, 123541, doi: [10.1103/PhysRevD.103.123541](https://doi.org/10.1103/PhysRevD.103.123541)
- Borhanian, S., & Sathyaprakash, B. S. 2022, arXiv e-prints, arXiv:2202.11048. <https://arxiv.org/abs/2202.11048>
- Cao, S., Liu, T., Biesiada, M., et al. 2022, *ApJ*, 926, 214, doi: [10.3847/1538-4357/ac4256](https://doi.org/10.3847/1538-4357/ac4256)
- Christensen, N. 2019, *RPPh*, 82, 016903, doi: [10.1088/1361-6633/aae6b5](https://doi.org/10.1088/1361-6633/aae6b5)
- Ciolfi, R., et al. 2021, *Exper. Astron.*, 52, 245, doi: [10.1007/s10686-021-09795-9](https://doi.org/10.1007/s10686-021-09795-9)

- Cutler, C., & Harms, J. 2006, *PhRvD*, 73, 042001, doi: [10.1103/PhysRevD.73.042001](https://doi.org/10.1103/PhysRevD.73.042001)
- Ding, X., Biesiada, M., & Zhu, Z.-H. 2015, *JCAP*, 12, 006, doi: [10.1088/1475-7516/2015/12/006](https://doi.org/10.1088/1475-7516/2015/12/006)
- Dominik, M., Belczynski, K., Fryer, C., et al. 2013, *ApJ*, 779, 72, doi: [10.1088/0004-637X/779/1/72](https://doi.org/10.1088/0004-637X/779/1/72)
- Dominik, M., Berti, E., O’Shaughnessy, R., et al. 2015, *ApJ*, 806, 263, doi: [10.1088/0004-637X/806/2/263](https://doi.org/10.1088/0004-637X/806/2/263)
- Finn, L. S. 1992, *PhRvD*, 46, 5236, doi: [10.1103/PhysRevD.46.5236](https://doi.org/10.1103/PhysRevD.46.5236)
- Gao, Y., Lai, X.-Y., Shao, L., & Xu, R.-X. 2022, *MNRAS*, 509, 2758, doi: [10.1093/mnras/stab3181](https://doi.org/10.1093/mnras/stab3181)
- Gardner, J. P., et al. 2006, *SSRv*, 123, 485, doi: [10.1007/s11214-006-8315-7](https://doi.org/10.1007/s11214-006-8315-7)
- Gehrels, N., et al. 2004, *ApJ*, 611, 1005, doi: [10.1086/422091](https://doi.org/10.1086/422091)
- Geng, S., Cao, S., Liu, T., et al. 2020, *ApJ*, 905, 54, doi: [10.3847/1538-4357/abc076](https://doi.org/10.3847/1538-4357/abc076)
- Graham, M. J., et al. 2019, *PASP*, 131, 078001, doi: [10.1088/1538-3873/ab006c](https://doi.org/10.1088/1538-3873/ab006c)
- Grover, K., Fairhurst, S., Farr, B. F., et al. 2014, *PhRvD*, 89, 042004, doi: [10.1103/PhysRevD.89.042004](https://doi.org/10.1103/PhysRevD.89.042004)
- Hild, S., et al. 2011, *CQGra*, 28, 094013, doi: [10.1088/0264-9381/28/9/094013](https://doi.org/10.1088/0264-9381/28/9/094013)
- Hooper, S., Chung, S. K., Luan, J., et al. 2012, *PhRvD*, 86, 024012, doi: [10.1103/PhysRevD.86.024012](https://doi.org/10.1103/PhysRevD.86.024012)
- in ’t Zand, J. J. M., et al. 2019, *Sci. China Phys. Mech. Astron.*, 62, 029506, doi: [10.1007/s11433-017-9186-1](https://doi.org/10.1007/s11433-017-9186-1)
- Isoyama, S., Nakano, H., & Nakamura, T. 2018, *PTEP*, 2018, 073E01, doi: [10.1093/ptep/pty078](https://doi.org/10.1093/ptep/pty078)
- Kalogera, V., Sathyaprakash, B. S., Bailes, M., et al. 2021, arXiv e-prints, arXiv:2111.06990. <https://arxiv.org/abs/2111.06990>
- Kawamura, S., et al. 2011, *CQGra*, 28, 094011, doi: [10.1088/0264-9381/28/9/094011](https://doi.org/10.1088/0264-9381/28/9/094011)
- . 2021, *PTEP*, 2021, 05A105, doi: [10.1093/ptep/ptab019](https://doi.org/10.1093/ptep/ptab019)
- Kudoh, H., Taruya, A., Hiramatsu, T., & Himemoto, Y. 2006, *PhRvD*, 73, 064006, doi: [10.1103/PhysRevD.73.064006](https://doi.org/10.1103/PhysRevD.73.064006)
- Lei, L., Li, J., Wu, J., Jiang, S., & Chen, B. 2021, *AR&T*, 18, L18, doi: [10.14005/j.cnki.issn1672-7673.20200713.001](https://doi.org/10.14005/j.cnki.issn1672-7673.20200713.001)
- Liu, C., & Shao, L. 2022, *ApJ*, 926, 158, doi: [10.3847/1538-4357/ac3cbf](https://doi.org/10.3847/1538-4357/ac3cbf)
- Liu, C., Shao, L., Zhao, J., & Gao, Y. 2020, *MNRAS*, 496, 182, doi: [10.1093/mnras/staa1512](https://doi.org/10.1093/mnras/staa1512)
- Madau, P., & Dickinson, M. 2014, *ARA&A*, 52, 415, doi: [10.1146/annurev-astro-081811-125615](https://doi.org/10.1146/annurev-astro-081811-125615)
- Magee, R., & Borhanian, S. 2022, arXiv e-prints, arXiv:2201.11841. <https://arxiv.org/abs/2201.11841>
- Mandel, I., & Broekgaarden, F. S. 2022, *LRR*, 25, 1, doi: [10.1007/s41114-021-00034-3](https://doi.org/10.1007/s41114-021-00034-3)
- Nakano, H., Fujita, R., Isoyama, S., & Sago, N. 2021, *Univ*, 7, 53, doi: [10.3390/universe7030053](https://doi.org/10.3390/universe7030053)
- Nitz, A. H., & Dal Canton, T. 2021, *ApJL*, 917, L27, doi: [10.3847/2041-8213/ac1a75](https://doi.org/10.3847/2041-8213/ac1a75)
- Nitz, A. H., Dal Canton, T., Davis, D., & Reyes, S. 2018, *PhRvD*, 98, 024050, doi: [10.1103/PhysRevD.98.024050](https://doi.org/10.1103/PhysRevD.98.024050)
- Phinney, E. S. 2001, arXiv e-prints, arXiv:astro. <https://arxiv.org/abs/astro-ph/0108028>
- Piórkowska-Kurpas, A., Hou, S., Biesiada, M., et al. 2021, *ApJ*, 908, 196, doi: [10.3847/1538-4357/abd482](https://doi.org/10.3847/1538-4357/abd482)
- Sachdev, S., et al. 2020, *ApJL*, 905, L25, doi: [10.3847/2041-8213/abc753](https://doi.org/10.3847/2041-8213/abc753)
- Sathyaprakash, B., et al. 2019, *BAAS*, 51, 251. <https://arxiv.org/abs/1903.09221>
- Schutz, B. F. 1986, *Natur*, 323, 310, doi: [10.1038/323310a0](https://doi.org/10.1038/323310a0)
- Sedda, M. A., et al. 2020, *CQGra*, 37, 215011, doi: [10.1088/1361-6382/abb5c1](https://doi.org/10.1088/1361-6382/abb5c1)
- . 2021, *ExA*, 51, 1427, doi: [10.1007/s10686-021-09713-z](https://doi.org/10.1007/s10686-021-09713-z)
- Seto, N., Kawamura, S., & Nakamura, T. 2001, *PhRvL*, 87, 221103, doi: [10.1103/PhysRevLett.87.221103](https://doi.org/10.1103/PhysRevLett.87.221103)
- Shi, D.-D., Zheng, X.-Z., Zhao, H.-B., et al. 2018, *AcASn*, 59, 1, doi: [10.15940/j.cnki.0001-5245.2018.03.001](https://doi.org/10.15940/j.cnki.0001-5245.2018.03.001)
- Singh, N., Bulik, T., Belczynski, K., & Askar, A. 2021, arXiv e-prints, arXiv:2112.04058. <https://arxiv.org/abs/2112.04058>
- Sun, H., Zhang, B., & Li, Z. 2015, *ApJ*, 812, 33, doi: [10.1088/0004-637X/812/1/33](https://doi.org/10.1088/0004-637X/812/1/33)
- Virgili, F. J., Zhang, B., O’Brien, P., & Troja, E. 2011, *ApJ*, 727, 109, doi: [10.1088/0004-637X/727/2/109](https://doi.org/10.1088/0004-637X/727/2/109)
- Wanderman, D., & Piran, T. 2015, *MNRAS*, 448, 3026, doi: [10.1093/mnras/stv123](https://doi.org/10.1093/mnras/stv123)
- Yagi, K., & Seto, N. 2011, *PhRvD*, 83, 044011, doi: [10.1103/PhysRevD.83.044011](https://doi.org/10.1103/PhysRevD.83.044011)
- Yuan, W., Zhang, C., Ling, Z., et al. 2018, in *Society of Photo-Optical Instrumentation Engineers (SPIE) Conference Series*, Vol. 10699, *Space Telescopes and Instrumentation 2018: Ultraviolet to Gamma Ray*, ed. J.-W. A. den Herder, S. Nikzad, & K. Nakazawa, 1069925, doi: [10.1117/12.2313358](https://doi.org/10.1117/12.2313358)
- Zhang, D.-L., et al. 2019, *NIMPA*, 921, 8, doi: [10.1016/j.nima.2018.12.032](https://doi.org/10.1016/j.nima.2018.12.032)
- Zhu, J.-P., et al. 2021, *ApJ*, 917, 24, doi: [10.3847/1538-4357/abfe5e](https://doi.org/10.3847/1538-4357/abfe5e)

## APPENDIX

**Table 3.** The values of  $\Omega_0^{\text{DCO}}$  (in the unit of  $10^{-12}$ ) in Eq. (B4) for different population models. The population models “Stan.High” and “Oce.High” for NSBHs and BBHs are taken from Dominik et al. (2013).

	BNS	NSBH	BBH
SFR14	4.15	–	–
LN	2.66	–	–
Stan.High	2.40	4.50	405
Oce.High	11.0	15.8	2227

## A. MERGER RATE CALCULATION

In models “SFR14” and “LN”, we assume that the BNS merger rate density evolves with redshift  $z$  via

$$\mathcal{R}(z) = \mathcal{R}_0 f(z), \quad (\text{A1})$$

where  $\mathcal{R}_0$  is the local merger rate and  $f(z)$  is the corresponding normalized (dimensionless) redshift distribution model. For models “Stan.High” and “Oce.High”, we use the  $\mathcal{R}(z)$  provided by Dominik et al. (2013) directly. The number of merger events up to redshift  $z_{\text{lim}}$  within a period  $T_{\text{obs}}$  can then be obtained with

$$N(z_{\text{lim}}) = T_{\text{obs}} \times \int_0^{z_{\text{lim}}} \frac{4\pi D_L^2(z) \mathcal{R}(z)}{(1+z)^3 H(z)} dz, \quad (\text{A2})$$

where  $T_{\text{obs}} = 20$  yr (i.e.,  $\sim 20 \times 52$  weeks),  $z_{\text{lim}} = 10$  by our choice, and  $H(z) \equiv H_0 \sqrt{\Omega_M(1+z)^3 + \Omega_\Lambda}$  is the Hubble parameter at redshift  $z$ .

## B. GW FOREGROUND FROM UNRESOLVED DCO SYSTEMS

At the decihertz band, a stochastic GW from DCOs is dominated by their inspiral stages, and characterized by its fractional energy density  $\Omega_{\text{GW}}$  per logarithmic frequency interval,

$$\Omega_{\text{GW}}(f) \equiv \frac{1}{\rho_c} \frac{d\rho_{\text{GW}}(f)}{d \ln f}, \quad (\text{B3})$$

where  $\rho_c = 3H_0^2/(8\pi)$  is the critical energy density of the Universe. The GW foreground by astrophysical compact binaries is given by (Phinney 2001)

$$\Omega_{\text{GW}}^{\text{DCO}}(f) = \frac{8\pi^{5/3}}{9} \frac{1}{H_0^2} \mathcal{M}^{5/3} f^{2/3} \int_0^\infty dz \frac{\mathcal{R}(z)}{(1+z)^{4/3} H(z)}. \quad (\text{B4})$$

Taking a specific population model and integrating Eq. (B4), one derives,

$$\Omega_{\text{GW}}^{\text{DCO}}(f) = \Omega_0^{\text{DCO}} \left( \frac{H_0}{67.4 \text{ km s}^{-1} \text{ Mpc}^{-1}} \right)^{-3} \left( \frac{\mathcal{M}}{\mathcal{M}_{\text{DCO}}} \right)^{5/3} \left( \frac{f}{1 \text{ Hz}} \right)^{2/3}, \quad (\text{B5})$$

where  $\mathcal{M}_{\text{DCO}}$  is the chirp mass of the sources in the population. We choose  $\mathcal{M}_{\text{BNS}} = 1.22 M_\odot$ ,  $\mathcal{M}_{\text{NSBH}} = 6.09 M_\odot$ , and  $\mathcal{M}_{\text{BBH}} = 24.5 M_\odot$  in the calculation. The  $\Omega_0^{\text{DCO}}$  for various population models are listed in Table 3.

The total GW foreground spectrum  $S_h$  is then

$$S_h^{\text{DCO}}(f) = \frac{4}{\pi} f^{-3} \rho_c \Omega_{\text{GW}}^{\text{DCO}}(f), \quad (\text{B6})$$

which is plotted as dotted grey lines in Fig. 2 for model “Stan.High”. The confusion noise of unresolved systems will then modify the noise spectrum of the detector via

$$S_n^{\text{total}}(f) = S_h^{\text{DCO}}(f) + S_n^{\text{instrument}}(f). \quad (\text{B7})$$

We use  $S_n^{\text{total}}$  to explore the effects of the confusion noise in Sec. 7.